Impact of Interface Charge on the Electrostatics of Field-Plate Assisted RESURF Devices

Boni K. Boksteen, *Student Member, IEEE*, Alessandro Ferrara, *Student Member, IEEE*, Anco Heringa, Peter G. Steeneken, and Raymond J. E. Hueting, *Senior Member, IEEE*

Abstract—A systematic study on the effects of arbitrary parasitic charge profiles, such as trapped or fixed charge, on the 2-D potential distribution in the drain extension of reverse-biased field-plate-assisted reduced surface field (RESURF) devices is presented. Using TCAD device simulations and analytical means, the significance of the so-called characteristic or natural length λ is highlighted with respect to the potential distribution and related phenomena in both ideal (virgin) and nonideal (degraded) extensions. Subsequently, a novel and easy-to-use charge-response method is introduced that enables calculation of the potential distribution for an arbitrary parasitic charge profile once the peak potential and lateral fall-off ($\propto \lambda$) caused by a single unit charge has been determined. This can be used for optimizing and predicting the performance, also after hot carrier injection, of RESURF power devices.

Index Terms—Electrostatics, FinFET, high-voltage, hot-carrier-induced charge injection (HCI), interface charge, junctionless transistor, reduced surface field (RESURF), SOI.

I. INTRODUCTION

PROPER shaping of the electric field distribution in the drain extension of power devices plays a key role in improving the specific ON-resistance versus breakdown voltage tradeoff. Through a delicate act of charge balancing, optimal lateral fields can be achieved at OFF-state or semi-ON-state (subthreshold) through different types of reduced surface field (RESURF) effects. Understandably a relatively small nonideality in this balance, such as interface charge, can cause changes in device characteristics which can lead to failure.

The focus of this paper is on devices where the RESURF effect is dominantly induced by field-plates (FPs), as found in many SOI or Trench-MOS-based technologies [1]–[8]. Fig. 1 shows the lateral field distribution and resulting (subthreshold) device characteristics in reverse-bias operation for: 1) a virgin
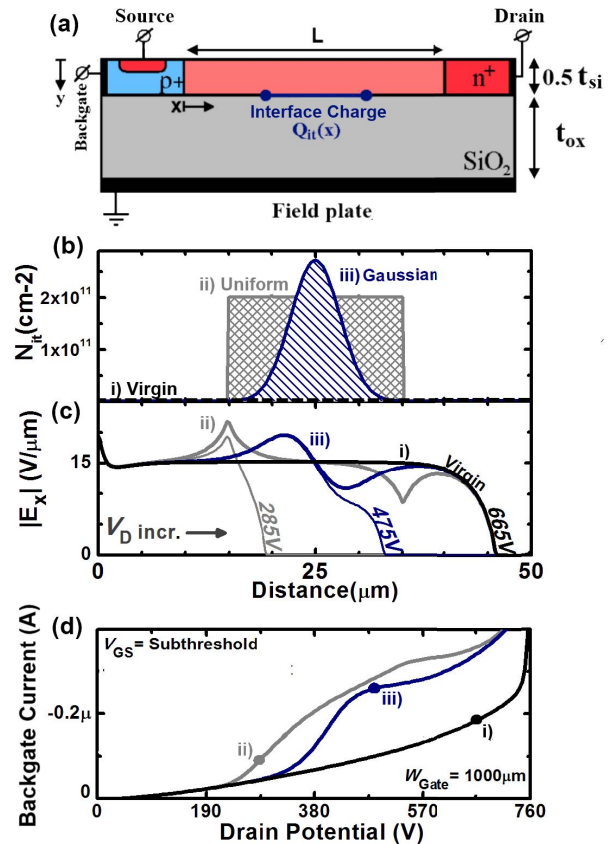
Fig. 1. Effect of interface charge on the reverse-bias operation of FP-assisted RESURF structures. (a) Schematic half-width cross section of the device, in which the axis of device symmetry is at $y = 0$, with interface charge (Q_{it}) indicated. (b) Fixed and Gaussian-shaped interface charge profiles ($N_{it}(x) = Q_{it}(x)/q$). (c) Virgin and degraded lateral fields. (d) Subthreshold I–V and breakdown behavior at the backgate (body) terminal.

device with ideal RESURF; 2) the device after degradation by a uniformly distributed interface charge profile; and 3) the device degraded by a Gaussian-shaped interface charge profile. The degraded devices contain interface charge along the drain extension at the Si/SiO$_2$ interface, as shown in Fig. 1(a).

For the ideal device 1), a uniform lateral field and a high breakdown voltage of ∼760 V is observed. When interface charge is introduced, in cases 2) and 3), a nonuniform field is obtained resulting in nonideal I–V curves with reduced breakdown voltages (BV). Since interface charge can lead to an electric field increase, hot-carrier-induced charge injection (HCI) is a reliability concern in RESURF devices [9]–[12].
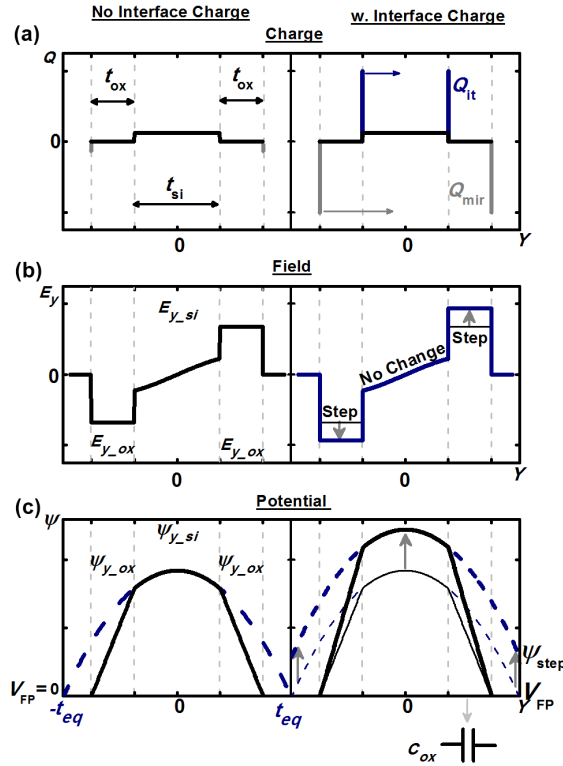
Fig. 2. Schematic vertical cross sections showing changes in (a) charge, (b) field, and (c) potential distributions in an ideal (left) and a degraded (right) drain extension. The arrows in (a) indicate the 1-D (field) step responses of the respective Dirac delta charges. Cross sections of the complete structure are presented, with the axis of symmetry at $y = 0$.

Physical understanding and models of the charge-induced changes in the electric field are therefore essential for the design of drain extensions that can withstand worst case scenario HCI phenomena. The objectives of this paper are to provide an intuitive method to study the effect of (non-ideal) interface charge on device characteristics [Fig. 1(b)–(d)], to model this and to clarify the significance of the geometry-related modeling term λ. Except for the physically larger dimensions, the electrostatics in field plated RESURF devices are quite similar to that observed in (multigate) FD-SOI, FinFETs, nanowires [13], and junctionless transistors [14], [15]. This makes many of the analysis techniques and methods described in this paper applicable to a variety of device types.

The rest of this paper is organized as follows. Section II focuses on the effect of interface charge on the 1-D electrostatics along a vertical cross section of the device. Section III introduces the geometry-related length λ, and its impact on the electrostatic device behavior. Section IV extends an existing quasi-2-D FP-assisted RESURF model [8], [16] to include interface charge, focuses on how this changes the 2-D electrostatics and how to model these changes for arbitrary N_{it} distributions. Finally, conclusions are drawn in Section V.

II. INTERFACE CHARGE—1-D ELECTROSTATICS

Treating the electrostatics in 1-D improves the understanding and modeling of RESURF devices [8]. Fig. 2 shows

a schematic overview of the charge, the electric field, and the potential along the vertical (y-) direction in fully depleted silicon with and without interface charge $Q_{it} (= q \cdot N_{it})$.

Since a positive Q_{it} is more common in electrically stressed N-drain extension devices the focus is on positive-type charge, with negative charge having an inverse effect. Along a vertical cross section, the interface charge Q_{it} can be modeled as a Dirac delta charge at the semiconductor/dielectric interface, here Si/SiO$_2$, as shown in Fig. 2(a). With fully depleted silicon, a mirror charge Q_{mir} is formed at the FP interface. The combined effect of these charges [see step responses, arrows in Fig. 2(a)] is an increased field in the oxide (E_y^{ox}) while the semiconductor field (E_y^{si}) does not change [Fig. 2(b)]. This results in an increased potential drop across the oxide (E_y^{ox}), and consequently an increase or offset (ψ_{step}) in the parabolic semiconductor potential [Fig. 2(c)]. This charge-induced potential offset is taken into account considering the capacitance $C_{ox}(= \varepsilon_{ox}/t_{ox})$ with $\psi_{step} = Q_{it}/C_{ox}$. This allows the Q_{it} influence to be included in the 2-D potential distribution using the RESURF model [8], [16] as shown in Section IV. The (y-direction) 1-D parabolic potential profile as observed in Fig. 2(c) forms a key approximation [17] in many quasi-2-D device models [16], [18], [19] with t_{eq} the equivalent length at which the parabolic potential (dashed lines) drops to the FP potential V_{FP} [8].

III. LATERAL DECAY CHARACTERISTIC

In Section II, the effect of interface charge was described using 1-D electrostatics. However, for correct modeling of the impact of a charge perturbation in a dielectric interfaced semiconductor structure, the 2-D Poisson equation in the drift region [Fig. 1(a)] has to be solved

$$\frac{\partial^2 \psi(x, y)}{\partial x^2} + \frac{\partial^2 \psi(x, y)}{\partial y^2} = -\frac{\rho(x, y)}{\varepsilon_{si}} \qquad (1)$$

with ρ the total charge density and ε_{si} the silicon dielectric constant. From (1), it can be derived (as shown in [16], [20], and [21]) that the lateral (x-direction) potential distribution has an exponential decay according to $e^{\pm x/\lambda}$. This decay length λ is a key geometric scaling parameter commonly referred to as the natural length [13] or device characteristic length [20]. Since this parameter has a strong impact on optimizing device design and modeling of the device electrostatics in both low [13], [18], [20] and high [8], [16] voltage devices, this section illustrates the different methods used to determine it. After this, in Section IV, the effect of a charge perturbation on the potential distribution will be discussed.

A. Determining the Characteristic Length λ

Three equivalent 2-D structures [Fig. 3(a)] have been simulated with TCAD [22] using a dielectric stack electrostatically similar to fully depleted Si ($\varepsilon = \varepsilon_{si}$) sandwiched between insulating dielectrics (SiO$_2$, $\varepsilon = \varepsilon_{ox}$). From potential perturbations within this system [Fig. 3(b) and (c)], the lateral exponential decay is studied.

Fig. 3(c) confirms that this decay is equal to $1/\lambda$ on a natural logarithmic scale. From the slope of these curves, we obtain

This article has been accepted for inclusion in a future issue of this journal. Content is final as presented, with the exception of pagination.

BOKSTEEN *et al.*: IMPACT OF INTERFACE CHARGE ON THE ELECTROSTATICS OF FP ASSISTED RESURF DEVICES 3
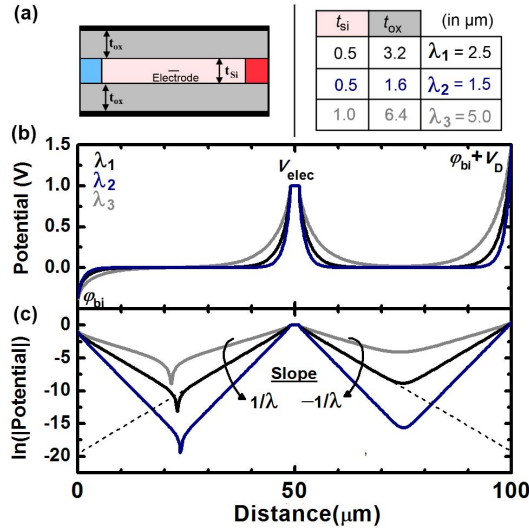

Fig. 3. TCAD obtained characteristic lengths λ for different vertical device dimensions. (a) Schematic cross section of simulated structures using an electrode biased at 1 V to study the potential decay. (b) and (c) Simulated lateral potential from: built-in p-n junction potential (left), electrode potential (center), and drain (biased at 1 V) potential (right).

TABLE I
DETERMINING λ ($k = \varepsilon_{si}/\varepsilon_{ox}$, η SEE REFERENCES)

Parabolic approx.	Evanescent mode
$\lambda = \sqrt{\frac{k}{\eta} \cdot t_{si} t_{ox}}$ [24]	$k \cdot \tan\left(\frac{t_{si}}{\lambda}\right) \tan\left(\frac{t_{ox}}{\lambda}\right) = 1$ [26] [20]
$\lambda = \sqrt{\frac{k}{\eta} \cdot t_{si} t_{ox} \left(1 + \frac{t_{si}}{4kt_{ox}}\right)}$ [16] [18]	$\lambda = \frac{t_{si} + 2kt_{ox}}{\pi}$ for ($t_{si} \gg t_{ox}$) [25]

$\lambda_1 = 2.5$ μm, $\lambda_2 = 1.5$ μm, and $\lambda_3 = 5.0$ μm. Hence, for smaller vertical dimensions the decay is steeper. In literature, several methods have been proposed to estimate λ. These methods can generally be divided into two main categories: 1) those based on relating the vertical potential distribution to the lateral decay using a parabolic [16], [18], [23], [24] potential approximation [Section II, Fig. 2(c)] and 2) those looking at the 2-D electrostatic problem of these systems using the evanescent-mode analysis [20], [25], [26]. The results from these are summarized in Table I.

Comparing λ values extracted from TCAD to those calculated using the equations in Table I shows that the methods based on the parabolic approximations underestimate λ. The implicit evanescent mode equation for λ does correctly determine the lateral fall-off (Fig. 4), albeit at the cost of much increased numerical complexity. Although the two groups of λ are used interchangeably as the lateral decay characteristic, from a mathematical standpoint they are in fact different quantities. The λ's determined by the evanescent mode analysis give the solution for the lateral fall-off [20], [25], [26], while the parabolic-approximation, as reported in [16] and [18], is accurate for determining fully depleted optimal device design at breakdown ($V_{DS} = V_{BV}$) conditions [8]. Even though in many situations, the parabolic approximated λ's are in good agreement [Fig. 4(a) for $t_{si} \gg t_{ox}$], it is recommended to use
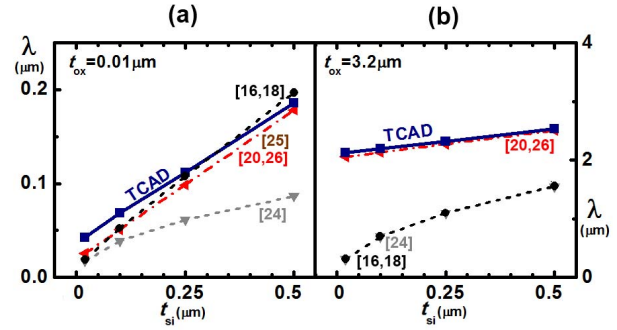

Fig. 4. Comparison of TCAD extracted λ values with those calculated using Table I. (a) $t_{si} \gg t_{ox}$. (b) $t_{si} \ll t_{ox}$.
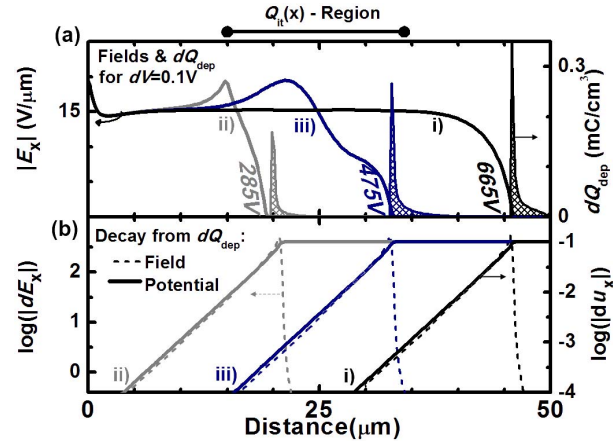

Fig. 5. TCAD results for a device with and without interface charge (as shown in Fig. 1). (a) Left axis: lateral field for different drain potentials, right axis: depletion charge perturbation induced by a voltage step $dV = 0.1$ V. The graded N-drift doping profile causes the increasing charge peak. (b) Decay of the field (left) and potential perturbation (right) in the depleted part of the drift extension caused by the depletion charge (dQ_{dep}).

an evanescent mode or TCAD determined λ to best model the lateral decay effects studied in this paper.

B. λ and Interface Charge

Using the parabolic potential approximation, the (ideal) drain extension of FP-assisted RESURF structures can be modeled as a symmetric FP/semiconductor structure [8]. The parabolic potential drop (toward V_{FP}) follows the equivalent depletion thickness t_{eq} as indicated by the dashed blue line in Fig. 2. For the latter, it holds that $t_{eq} = \sqrt{2}\lambda$. As shown in Section II, according to the 1-D equivalent model, interface charge does not affect t_{eq} (and hence λ) as the potential curvature is constant while only introducing an increase in V_{FP} equal to ψ_{step}.

To verify whether the lateral exponential decay is indeed unaffected by interface charge (Q_{it}), TCAD simulations have been performed. Fig. 5 shows the simulation results of both the lateral field and the potential induced by a depletion charge perturbation (dQ_{dep}), caused by a drain potential step of 0.1 V. This has been done for the different Q_{it} profiles shown in Fig. 1(b), that is: 1) no Q_{it} (ideal device); 2) a uniform; and 3) a Gaussian Q_{it} distribution. The constant decay ($\propto 1/\lambda$) in

Fig. 5(b) indicates that λ is a function of the device geometry and is not affected by the interface charge. This simplifies modeling of the effect of interface charge on the electrostatics, as will be discussed in Section IV.

IV. MODELING THE INTERFACE CHARGE

To assess degradation phenomena it should be known how interface charge affects the device electrostatics. In [8] and [16], the 2-D Poisson equation (1) was solved for (ideal) RESURF devices assuming a uniform lateral field, i.e., $d^2\psi(x,y)/dx^2 = d^2u(x)/dx^2 = 0$. The term $u(x)$ represents the lateral potential distribution at the potential line of symmetry ($t_{si}/2$ for symmetric, t_{si} for single sided devices [8]), the location of interest for subthreshold multiplication [Fig. 1(d)], [11], [27] and many other modeling purposes, e.g., subthreshold current [21] and threshold voltage [19] in junctionless transistors. This paper extends the solution of $u(x)$ [8], [16] by adding the potential offset caused by the interface charge (ψ_{step}, Section II) to that of the FP (V_{FP}) potential [Fig. 2(c)] resulting in the following equation:

$$\frac{d^2u(x)}{dx^2} - \frac{u(x) - (V_{FP} + \frac{qN_{it}}{C_{ox}})}{\lambda^2} = -\frac{\rho}{\varepsilon_s} \quad (2)$$

assuming the potential distribution can be described as $\psi(x,y) = u(x) \cdot g(y)$, with $u(x)$ and $g(y)$ dependent upon the lateral and vertical direction, respectively. The interface charge component is $Q_{it} = qN_{it}$, C_{ox} is the oxide capacitance per unit area, V_{FP} is the FP potential and $\rho = qN_D$ is the drift doping charge density. Since modeling the electrostatic perturbations (Δ's) caused by interface charge is the focus of this paper, the lateral potential $u(x)$ is split into

$$u(x) = u_{opt}(x) + \Delta u_{it}(x) \quad (3)$$

with u_{opt} the ideal lateral potential and Δu_{it} the potential caused by interface charge only. Subsequently, substituting this expression in (2) yields

$$\frac{d^2u_{opt}(x)}{dx^2} - \frac{u_{opt}(x) - V_{FP}}{\lambda^2} = -\frac{\rho}{\varepsilon_s} \quad (4a)$$

$$\frac{d^2\Delta u_{it}(x)}{dx^2} - \frac{\Delta u_{it}(x) - \frac{qN_{it}}{C_{ox}}}{\lambda^2} = 0 \quad (4b)$$

with (4a) giving the lateral potential distribution in the drift region in the absence of interface charge ($u(x) = u_{opt}(x)$). The potential perturbation ($\Delta u_{it}(x)$) will satisfy (4b), which can be rewritten as the more conventional nonhomogeneous differential equation

$$\frac{d^2\Delta u_{it}(x)}{dx^2} - \frac{\Delta u_{it(x)}}{\lambda^2} = -\frac{qN_{it}}{\lambda^2 C_{ox}}. \quad (5)$$

The shape of perturbation $\Delta u_{it}(x)$ can be derived using (5) with boundary conditions $\Delta u_{it}(0) = 0$ and $\Delta u_{it}(L) = 0$, where L is the length of the fully depleted drain extension and $x = 0$ is the position of the body-drain junction, see also Fig. 1(a). Notice that the same approach can be used to determine the potential perturbations caused by arbitrary biased separate FPs by replacing qN_{it}/C_{ox} with V_{FP}. Solving (5) in the regions of the drift extension without interface

charge results in a homogeneous ($N_{it} = 0$ cm^{-2}) differential equation with general solution

$$\Delta u_{it}(x) = A^+e^{\frac{x}{\lambda}} + A^-e^{-\frac{x}{\lambda}}. \quad (6)$$

For a single, delta-function-shaped interface charge $N_{it}(x) = \delta(x - x_0)$ at a position $x = x_0$, the analytical solution can be written in two parts

$$\Delta u_{\delta it,0}(x) = \begin{cases} u_{it,l}(x) = A_{l,0}^+ e^{\frac{x-x_0}{\lambda}} + A_{l,0}^- e^{-\frac{x-x_0}{\lambda}}, & x < x_0 \\ u_{it,r}(x) = A_{r,0}^+ e^{\frac{x-x_0}{\lambda}} + A_{r,0}^- e^{-\frac{x-x_0}{\lambda}}, & x > x_0 \end{cases} \quad (7)$$

with $u_{it,l}(x)$ on the left and $u_{it,r}(x)$ on the right side of the interface charge. The potential needs to be continuous and the condition for its derivative is obtained by integrating (5) over an infinitesimal distance that contains x_0. Thus, we obtain

$$u_{it,l}(x_0) = u_{it,r}(x_0) \quad (8)$$

$$\frac{du_{it,r}}{dx}(x_0) - \frac{du_{it,l}}{dx}(x_0) = -\frac{q}{\lambda^2 C_{ox}}. \quad (9)$$

From (9) it is clear that the analytical solution of u_{it} indeed has to be written in two parts to accurately model the discontinuity in its first derivative. In combination with the boundary conditions $\Delta u_{it}(0) = 0$ and $\Delta u_{it}(L) = 0$, the coefficients A are given by

$$A_{l,0}^- = \frac{q(1 - e^{2(L-x_0)/\lambda})}{2\lambda C_{ox}(e^{2L/\lambda} - 1)} \quad (10)$$

$$A_{l,0}^+ = -A_{l,0}^- e^{2x_0/\lambda} \quad (11)$$

$$A_{r,0}^- = A_{l,0}^- + \frac{q}{2\lambda C_{ox}} \quad (12)$$

$$A_{r,0}^+ = A_{l,0}^+ - \frac{q}{2\lambda C_{ox}}. \quad (13)$$

From (7) using the corresponding coefficients A_i it can be seen that the resultant (left, right) lateral fall-off for charges at different positions x_0 is related to the distance from the potential boundaries $x = 0$ and $x = L$. Having solved the equation for a single delta charge at position x_0, we can generalize the solution for any charge distribution in a window W_{it} by a set of delta charges at N positions x_i with $i = 0, 1, \ldots N - 1$, hence, $W_{it} = N \cdot (x_{i+1} - x_i)$. Each of the charges induces a potential contribution $\Delta u_{\delta it,i}(x)$, which needs to satisfy (5), such that the discrete convolution

$$\Delta u_{it}(x) = \sum_{i=0}^{N-1} \Delta u_{\delta it,i}(x) \quad (14)$$

$$= \sum_{i=0}^{N-1} \left(A_{l|r,i}^+ e^{\frac{x-x_i}{\lambda}} + A_{l|r,i}^- e^{-\frac{x-x_i}{\lambda}} \right) \quad (15)$$

holds. The values of the parameters A_i are different on the left and right side of each of the charges, satisfying (10)–(13). With these equations, the effect of an arbitrarily distributed charge on the potential distribution of a (RESURF) device can be calculated in a straightforward manner. Equation (15) can also be written as a more general convolution integral and its corresponding Laplace transform according to

$$\Delta u_{it}(x) = \mathscr{L}^{-1}\{N_{it}(s) \times \Delta u_{\delta it}(s)\} = [N_{it} * \Delta u_{\delta it}](x)$$

$$= \int_0^x N_{it}(\tau) \cdot \Delta u_{\delta it}(x - \tau)d\tau. \quad (16)$$

Fig. 7. (a) 1-μm wide interface charge windows W_{it} used in TCAD simulations. Effect of the respective interface charge windows on (b) the potential $\Delta u_{it}(x)$ and (c) lateral field $\Delta E_{it}(x)$ for increasing N_{it} with a fixed interface charge window of 1 μm. (d) I–V curves formed by impact ionization for various N_{it} values. The lateral field peak increases with N_{it}, eventually causing premature local avalanche breakdown.
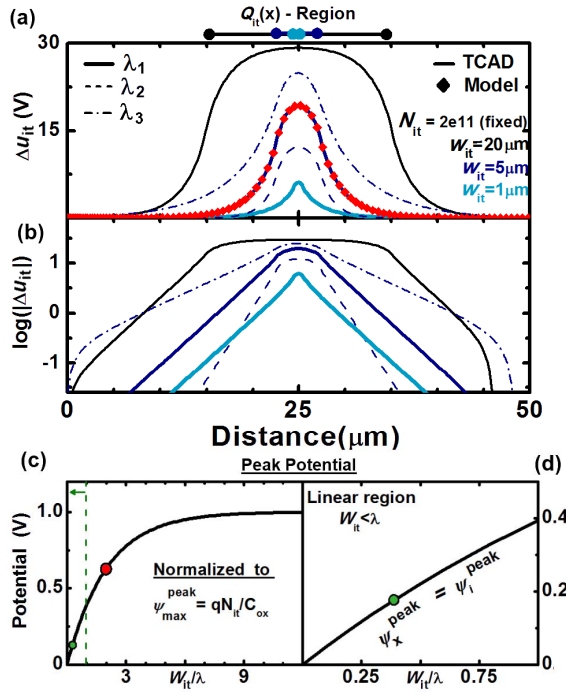
Fig. 6. Potential distribution caused by varying fixed N_{it} windows. (a) Linear, (b) logarithmic, and (c) normalized ψ_x^{peak} for increasing W_{it} and different λ's. A linear region is observed left of the vertical dashed line. (d) Linear region of $\psi_x^{peak} = \psi_i^{peak}$. The green dot indicates a W_{it}/λ that is usable for effective discretization using (15) and (19). The red dot indicates a W_{it}/λ that is not.

Finally, it is interesting to note that the introduced perturbation approach is generally applicable to devices with arbitrary, not necessarily RESURF optimized ($u_{opt}(x)$), potential distributions.

A. Potential Distribution Change for Windows of Fixed Q_{it}

Various device extensions [i.e., λ_1, λ_2, and λ_3, Fig. 3(a)] have been TCAD simulated using a interface charge of $q \times 2 \cdot 10^{11} = 32$ nC $\cdot$ cm^{-2} for varying window widths W_{it}. The ideal potential (and lateral field) distributions [Fig. 1(c), situation i] have been subtracted from the nonideal ones [see (3)] yielding the TCAD obtained changes in potential as shown in Fig. 6(a) and (b). These changes have also been modeled using (15) for comparison showing good agreement [Fig. 6(a)].

For a fixed λ and increasing window of interface charge [$W_{it} = 1, 5, 20$ μm, Fig. 6(a) and (b)] an increase in peak potential (ψ_x^{peak}) is seen. For a fixed window of interface charge [$W_{it} = 5$ μm, Fig. 6(a) and (b)], devices with smaller vertical (oxide) dimensions [smaller λ, Fig. 3(a)] and therefore larger oxide capacitances (C_{ox}) show a lower peak potential (ψ_x^{peak}). The normalized ψ_x^{peak} response versus W_{it}/λ is shown in Fig. 6(c). The mathematical description of this behavior can be obtained using the convolution integral (16) for the potential at $W_{it}/2$ resulting in

$$\psi_x^{peak}(W_{it}) = \frac{q N_{it}}{C_{ox}}\left(1 - e^{-\frac{W_{it}}{2\lambda}}\right) \quad (17)$$

which saturates to the 1-D value ($\psi_{step} = q \cdot N_{it}/C_{ox}$), described in Section II, for $W_{it} \gg \lambda$. This emphasizes that the 1-D approach for calculating the potential change caused by
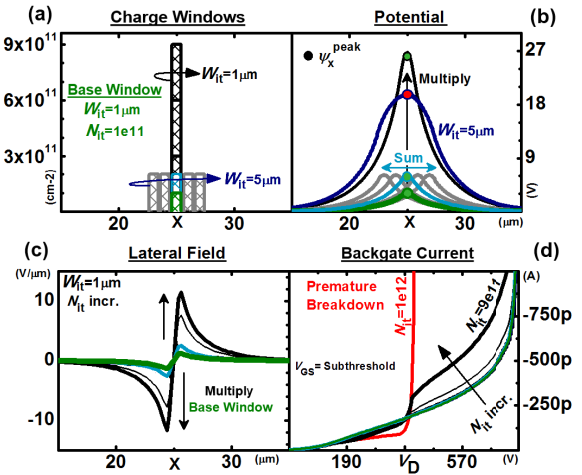
N_{it} does not hold laterally. On the other hand, for $W_{it,i} \ll \lambda$ ($W_{it,i} \approx dx$) the peak potential response will approach that of the delta function described in (7)–(13) at $x = x_i$ where the peak potential is given by

$$\psi_x^{peak}(W_{it,i}) = \psi_i^{peak} = \Delta u_{\delta it}(x_i) = A_{r,i}^+ + A_{r,i}^- = A_{l,i}^+ + A_{l,i}^-. \quad (18)$$

For the sake of convenience, we simplify (7) and (10)–(13) into a more compact form

$$\Delta u_{it,i}(x) = \begin{cases} \psi_i^{peak} \cdot \dfrac{\sinh(x/\lambda)}{\sinh(x_i/\lambda)} & x \leq x_i \\ \psi_i^{peak} \cdot \dfrac{\sinh((W-x)/\lambda)}{\sinh((W-x_i)/\lambda)} & x > x_i \\ 0 & x < 0 \vee x > W \end{cases} \quad (19)$$

with W being the depletion edge (see Section IV-C). The potential boundary conditions used to obtain the above are $\psi(x_i, t_{si}/2) = \psi_i^{peak}$, $\partial\psi/\partial y(x,0) = 0$, $\psi(0, y) = 0$, and $\psi(W, y) = 0$. Fig. 8(a)–(c) shows modeling the (potential) response using (17) and (19). The field can be obtained through differentiation of the potential, $\Delta E_{it}(x) = -du_{it}(x)/dx$. Equation (19) does not include the lateral drop in potential within the charge window [Figs. 6(a) and 7(b)]. It simply models the response as a peak potential, located at the center of the window, with a lateral exponential drop on each side of $e^{-x/\lambda}$, respectively, $e^{x/\lambda}$. As such, (19) is only valid when the charge window is sufficiently narrow such that the lateral potential drop within the window is negligible.

The discretization method (15) has been verified with TCAD simulations using relatively narrow windows of 1 μm ($W_{it,i} < \lambda$) to construct the potential and field response of wider charge windows. Some results are shown in Fig. 7 where a single (base) window response in the linear region of Fig. 6(c) and (d) ($N_{it} = 1 \cdot 10^{11}$ cm^{-2}, $W_{it} = 1$ μm) enables the reproduction of other responses through a simple multiplication (green dot, $N_{it} = 9 \cdot 10^{11}$ cm^{-2}) or summation

6

This article has been accepted for inclusion in a future issue of this journal. Content is final as presented, with the exception of pagination.
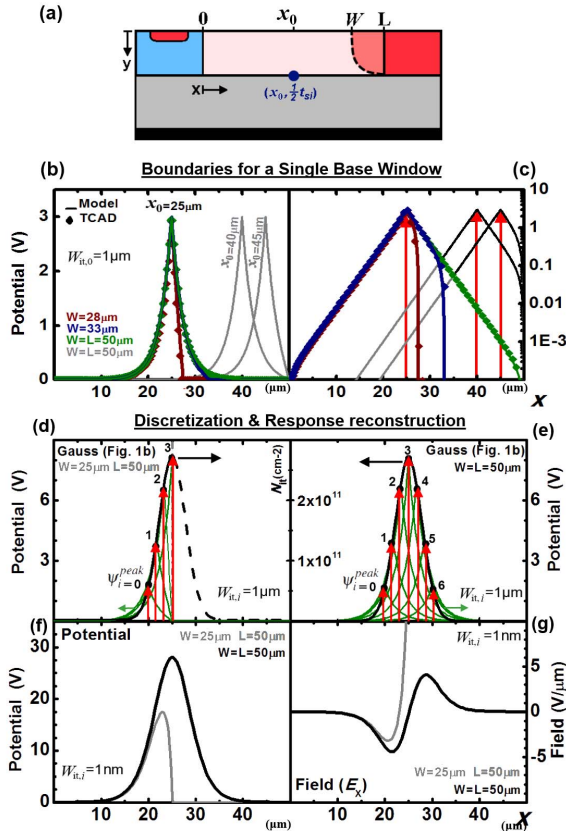
IEEE TRANSACTIONS ON ELECTRON DEVICES

Fig. 8. (a) Device cross section illustrating a unit (δ, red arrows) interface charge window for laterally partially ($W < L$) and fully ($W = L$) depleted drain extensions. (b) and (c) TCAD obtained and modeled $\Delta u_{it}(x)$ for partially and fully depleted drain extensions. (d) and (e) Discretization of the Gaussian shaped $N_{it}(x)$ distribution in unit windows (δ's) of charge (red arrows) with their respective potential (green lines). (f) Total potential. (g) Field ($\Delta u_{it}(x)$, $\Delta E_{it}(x)$) obtained through summation (15) of the separate responses ($W_{it} = 1$ μm) for both the partially (gray, $W = 25$ μm, $L = 50\mu$m) and fully (black, $W = L = 50$ μm) depleted case.

(red dot, $W_{it} = 5$ μm). On the other hand, a 5-μm window ($W_{it,i} > \lambda$) as a base window [red dot, Fig. 6(c)] is not sufficiently narrow for effective construction using (14) and (19).

B. Effect of Interface Charge on Device Characteristics

Changes in lateral field, e.g., caused by interface charge, affect the impact ionization multiplication resulting in a change of the subthreshold device I–V characteristics [Fig. 7(c) and (d)]. When the absolute value of the lateral field change $\Delta E_{it}(x)$ caused by a nonideality is as high as the lateral field E_x, local breakdown (red line), at this critical peak field location, will occur. Since the lateral field for the device treated here is 15 V/μm [Fig. 1(b)] and the base interface charge window causes a lateral field change of ~1.3 V/μm the avalanche breakdown seen for a 1-μm wide N_{it} of $1.2 \cdot 10^{11}$ cm^{-2} [Fig. 7(d)] can be explained, as this is 12 times the base window charge causing a local critical (12 × 1.3 V/μm) field peak in $\Delta E_{it}(x)$.

C. Discretization of N_{it} and Partially Depleted Modeling

To determine multiplication [8] at each drain bias value in OFF-state or subthreshold, the field and potential response at
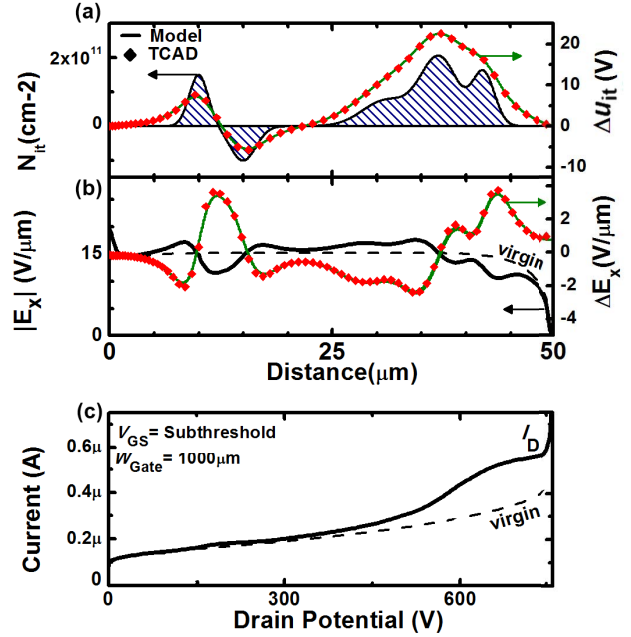

Fig. 9. TCAD simulation and perturbation modeling results for an arbitrary interface charge profile using the device [Fig. 3(a)] with $\lambda = 2.5$ μm. (a) Left axis: interface charge profile, right axis: potential response $\Delta u_{it}(x)$. (b) Total (E_x, left axis) and change [$\Delta E_{it}(x)$, right axis] in field response. (c) Subthreshold I–V behavior. The results obtained for the ideal device are indicated by dashed lines, while the degraded device is indicated by the solid lines.

different depletion widths is required. This necessitates the modeling of partially depleted drift extensions ($W < L$), which can be done by changing the boundary condition $\psi(L, y) = 0$ to $\psi(W, y) = 0$ and applying the discrete convolution of (14) together with (19). Fig. 8(b) and (c) shows a selection of different boundary conditions and positions (x_i) for a single base window of charge, while Fig. 8(d)–(g) shows the response of the full Gaussian N_{it} distribution of Fig. 1(c) using (14), (17), and (19) at two different depletion widths ($W = 25$ μm and $W = 50$ μm $= L$). For any form of discretization, the narrower the discretization window the better the modeled response. The base discretization window used in Fig. 8(b)–(e) was 1-μm wide for ease of illustration, for better response modeling, however, the results shown in Fig. 8(f) and (g) and 9 are obtained using a much narrower base window width W_{it} of 1 nm.

D. Field Distribution of an Arbitrary N_{it} Profile

The proposed method is applied to an arbitrary interface charge distribution (with both positive and negative N_{it}) and compared with TCAD simulations. Using the appropriate λ (Section III), excellent agreement is achieved [Fig. 9(a)]. By adding the field distributions for a virgin case (E_x^{virgin}, e.g., obtained with the analytical models presented in [8] and [16]) to the $\Delta E_{it}(x)$ caused by the interface charge, the total field distributions E_x can be obtained as shown in Fig. 9(b). With this resultant field distribution, the drain potential can be obtained through integration of the field ($V_{DS} = -\int_0^W E_x(x)dx$). The subthreshold I–V [Fig. 9(c)] obtained using the E_x dominated impact ionization multiplication as described in [8] shows that interface charge will in fact affect

This article has been accepted for inclusion in a future issue of this journal. Content is final as presented, with the exception of pagination.

BOKSTEEN *et al.*: IMPACT OF INTERFACE CHARGE ON THE ELECTROSTATICS OF FP ASSISTED RESURF DEVICES 7

the $I-V$ behavior. In addition, changes in $I-V$ characteristics caused by arbitrarily biased separate FPs along the drain extension can be obtained by changing the field plate potential according to $V_{\mathrm{FP}}(x) = \psi_{\mathrm{step}}(x) = q N_{\mathrm{it}}(x)/C_{\mathrm{ox}}$ (see Section II). Because of this analogy in influence, device structures with separately biased FPs can be used to investigate and or suppress $[V_{\mathrm{FP}}(x) = -q N_{\mathrm{it}}(x)/C_{\mathrm{ox}}, (2)]$ the influence of interface charge.

V. CONCLUSION

In this paper, a systematic study on the effects of arbitrary parasitic charge profiles on the 2-D potential distribution in the drain extension of FP-assisted RESURF devices is presented. The importance of the device characteristic length λ in dielectric-interfaced (depleted) semiconductor systems is shown. A powerful charge-response method is introduced, requiring only (14), (17), and (19) for reconstructing the electrostatic response of an arbitrary parasitic charge distribution. This method can be used for optimizing and predicting the performance of FP-assisted RESURF devices while providing a valuable step toward the development of a universal HCI model.

REFERENCES

[1] S. Merchant, E. Arnold, H. Baumgart, S. Mukherjee, H. Pein, and R. Pinker, "Realization of high breakdown voltage ($> 700V$) in thin SOI devices," in *Proc. ISPSD*, 1991, pp. 31–35.
[2] S. Mahalingam and B. J. Baliga, "A low forward drop high voltage trench MOS barrier Schottky rectifier with linearly graded doping profile," in *Proc. ISPSD*, 1998, pp. 187–190.
[3] Y.-K. Leung, A. K. Paul, J. D. Plummer, and S. S. Wong, "Lateral IGBT in thin SOI for high voltage, high speed power IC," *IEEE Trans. Electron Devices*, vol. 45, no. 10, pp. 2251–2254, Oct. 1998.
[4] G. E. J. Koops, E. A. Hijzen, R. J. E. Hueting, and M. A. A. Zandt, "RESURF stepped oxide (RSO) MOSFET for 85V having a record-low specific on-resistance," in *Proc. ISPSD*, 2004, pp. 185–188.
[5] J. Sonsky and A. Heringa, "Dielectric resurf: Breakdown voltage control by STI layout in standard CMOS," in *IEEE IEDM Tech. Dig.*, Dec. 2005, pp. 372–376.
[6] P. Moens *et al.*, "XtreMOS : The first integrated power transistor breaking the silicon limit," in *Proc. IEEE IEDM*, Dec. 2006, pp. 1–4.
[7] Y. Chen, Y. C. Liang, and G. S. Samudra, "Design of gradient oxide-bypassed superjunction power MOSFET devices," *IEEE Trans. Power Electron.*, vol. 22, no. 4, pp. 1303–1310, Jul. 2007.
[8] B. K. Boksteen, A. Ferrara, A. Heringa, P. G. Steeneken, G. E. J. Koops, and R. J. E. Hueting, "Design optimization of field-plate assisted RESURF devices," in *Proc. ISPSD*, 2013, pp. 237–240.
[9] D. Varghese *et al.*, "Off-state degradation in drain-extended nMOS transistors: Interface damage and correlation to dielectric breakdown," *IEEE Trans. Electron Devices*, vol. 54, no. 10, pp. 2669–2678, Oct. 2007.
[10] P. Moens, D. Varghese, and M. Alam, "Towards a universal model for hot carrier degradation in DMOS transistors," in *Proc. ISPSD*, 2010, pp. 61–64.
[11] B. K. Boksteen *et al.*, "On the degradation of field-plate assisted RESURF power devices," in *Proc. IEEE IEDM*, Dec. 2012, pp. 13.4.1–13.4.4.
[12] S. Reggiani *et al.*, "TCAD simulation of hot-carrier and thermal degradation in STI-LDMOS transistors," *IEEE Trans. Electron Devices*, vol. 60, no. 2, pp. 691–698, Feb. 2013.
[13] J. Colinge, *FinFETS and Other Multi-Gate Transistors*. New York, NY, USA: Springer-Verlag, 2008.
[14] J.-H. Woo, J.-M. Choi, and Y.-K. Choi, "Analytical threshold voltage model of junctionless double-gate MOSFETs with localized charges," *IEEE Trans. Electron Devices*, vol. 60, no. 9, pp. 2951–2955, Sep. 2013.
[15] J.-P. Colinge *et al.*, "Reduced electric field in junctionless transistors," *Appl. Phys. Lett.*, vol. 96, no. 7, p. 073510, 2010.
[16] S. Merchant, "Analytical model for the electric field distribution in SOI RESURF and TMBS structures," *IEEE Trans. Electron Devices*, vol. 46, no. 6, pp. 1264–1267, Jun. 1999.

[17] K. K. Young, "Analysis of conduction in fully depleted SOI MOSFETs," *IEEE Trans. Electron Devices*, vol. 36, no. 3, pp. 504–506, Mar. 1989.
[18] K. Suzuki, T. Tanaka, Y. Tosaka, H. Horie, and Y. Arimoto, "Scaling theory for double-gate SOI MOSFETs," *IEEE Trans. Electron Devices*, vol. 40, no. 12, pp. 2326–2329, Dec. 1993.
[19] T.-K. Chiang, "A quasi-two-dimensional threshold voltage model for short-channel junctionless double-gate MOSFETs," *IEEE Trans. Electron Devices*, vol. 59, no. 9, pp. 2284–2289, Sep. 2012.
[20] S.-H. Oh, D. Monroe, and J. M. Hergenrother, "Analytic description of short-channel effects in fully-depleted double-gate and cylindrical, surrounding-gate MOSFETs," *IEEE Electron Device Lett.*, vol. 21, no. 9, pp. 445–447, Sep. 2000.
[21] A. Gnudi, S. Reggiani, E. Gnani, and G. Baccarani, "Semianalytical model of the subthreshold current in short-channel junctionless symmetric double-gate field-effect transistors," *IEEE Trans. Electron Dev.*, vol. 60, no. 4, pp. 1342–1348, Apr. 2013.
[22] *ATLAS (Version: 5.18.3.R)* Silvaco Inc, Santa Clara, CA, USA. Mar. 2012
[23] K. Young, "Short-channel effect in fully depleted SOI MOSFETs," *IEEE Trans. Electron Devices*, vol. 36, no. 2, pp. 399–402, Feb. 1989.
[24] R.-H. Yan, A. Ourmazd, and K. F. Lee, "Scaling the Si MOSFET: From bulk to SOI to bulk," *IEEE Trans. Electron Devices*, vol. 39, no. 7, pp. 1704–1710, Jul. 1992.
[25] D. Monroe and J. M. Hergenrother, "Evanescent-mode analysis of short-channel effects in fully depleted SOI and related MOSFETs," in *Proc. IEEE Int. SOI Conf.*, Oct. 1998, pp. 157–158.
[26] D. J. Frank, Y. Taur, and H.-S. Wong, "Generalized scale length for two-dimensional effects in MOSFETs," *IEEE Trans. Electron Devices*, vol. 19, no. 10, pp. 385–387, Oct. 1998.
[27] R. van Dalen, A. Heringa, P. W. M. Boos, A. B. van der Wal, and M. J. Swanenberg, "Using multiplication to evaluate HCI degradation in HV-SOI devices," in *Proc. ISPSD*, 2010, pp. 89–92.

Boni K. Boksteen (S'10) received the M.Sc. (*cum laude*) degree in electrical engineering from the University of Twente, Enschede, The Netherlands, in 2010, where he is currently pursuing the Ph.D. degree.

He is currently involved in RESURF-based power MOS optimization and reliability with the University of Twente in collaboration with NXP Semiconductors, Eindhoven, The Netherlands.

Alessandro Ferrara (S'12) received the master's (*cum laude*) degree in electronic engineering from the Federico II University of Naples, Naples, Italy, in 2011. He is currently pursuing the Ph.D. degree with the University of Twente, Enschede, The Netherlands.

He is currently involved in power MOS reliability with the University of Twente in collaboration with NXP Semiconductors, Eindhoven, The Netherlands.

Anco Heringa received the degree from The University of Groningen, Groningen, The Netherlands, in 1977.

He was then involved in cardiophysics research at the Radboud University Nijmegen. He was a Consultant in process/device modeling at Philips, Eindhoven, The Netherlands, until 2002. He is currently with NXP Semiconductors, Eindhoven, where he is involved in integrated high-voltage devices.

Peter G. Steeneken received the M.Sc. (*cum laude*) and Ph.D. degrees in physics from the University of Groningen, Groningen, The Netherlands, in 1997 and 2002, respectively.

He has been at Philips and NXP Semiconductors, Eindhoven, The Netherlands, since 2002, where he studies and develops microelectromechanical devices and power transistors. He is currently a part-time Professor of Applied Nanophysics with the Delft University of Technology, Delft, The Netherlands.

Raymond J. E. Hueting (S'94–M'98–SM'06) received the M.Sc. (*cum laude*) and Ph.D. degrees in electrical engineering from the Delft University of Technology, Delft, The Netherlands.

He joined the Semiconductor Components Group at the University of Twente, Enschede, The Netherlands, in 2005, where he is involved in semiconductor device physics and modeling.